

# Comparison of the Theoretical and Experimental Performance of an Annular Helicon Plasma Source

IEPC-2007-236

Presented at the 30<sup>th</sup> International Electric Propulsion Conference, Florence, Italy  
September 17-20, 2007

Cengiz B. Akinli<sup>\*</sup>, Douglas D. Palmer<sup>†</sup>, and Mitchell L. R. Walker II<sup>‡</sup>  
Georgia Institute of Technology, Atlanta, GA, 30332, USA

**Abstract:** The Georgia Institute of Technology has created a nominally 1-kW annular helicon plasma source, derived the general helicon dispersion equations for an annular source, identified the first mode shape, performed power deposition calculations, and conducted parametric studies. The theoretical results are compared to experimental measurements of the electron temperature and number density in the annular helicon plasma over a range of applied RF forward power and radial locations. In particular, the results of radial plasma density profiles are compared to the theoretical model to confirm the validity of assumptions used. Initial results suggest that the density profile used as input to the theoretical model is reasonable. Profiles of electron density across a range of RF input power are consistent with theory and previous experimental results.

## Nomenclature

|             |   |  |
|-------------|---|--|
| $A_p$       | = | Langmuir probe collection area   |
| $a$         | = | annulus inner diameter   |
| $b$         | = | annulus outer diameter   |
| $c$         | = | speed of light   |
| $B$         | = | perturbed magnetic field   |
| $B_0$       | = | equilibrium magnetic field   |
| $e$         | = | electron charge  |
| HET         | = | Hall effect thruster   |
| $E$         | = | perturbed electric field   |
| $I_{es}$    | = | electron saturation current  |
| $I_p$       | = | Langmuir probe current   |
| $I_{sp}$    | = | specific impulse   |
| $j$         | = | perturbed current density  |
| $j_{\perp}$ | = | component of perturbed current density perpendicular to magnetic field |
| $k$         | = | axial wave number  |
| $r$         | = | radial displacement from helicon axis                                  |
| $m$         | = | azimuthal wave mode  |
| $n_0$       | = | equilibrium plasma density   |
| OML         | = | Orbital Motion Limited   |
| $r_p$       | = | Langmuir probe primary electrode radius                                |
| $T/P$       | = | thrust-to-power  |
| $T_e$       | = | electron temperature   |

---

<sup>\*</sup> Graduate Student, School of Aerospace Engineering, cakinli@gatech.edu

<sup>†</sup> Graduate Student, School of Aerospace Engineering, dougpalmer@gatech.edu

<sup>‡</sup> Assistant Professor, School of Aerospace Engineering, mitchell.walker@ae.gatech.edu

|               |   |  |
|---------------|---|--|
| $t$           | = | time   |
| USAF          | = | United States Air Force                        |
| VTF           | = | Vacuum Test Facility                           |
| $V_f$         | = | floating potential                             |
| $V_s$         | = | space potential                                |
| $V_p$         | = | Langmuir probe primary electrode voltage       |
| $z$           | = | axial displacement along helicon               |
| $Z_m$         | = | root of the m-order Bessel function            |
| $\beta$       | = | ratio of Langmuir probe tip to Debye length    |
| $\theta$      | = | angular displacement azimuthal to helicon axis |
| $\lambda_D$   | = | Debye length                                   |
| $\mu_0$       | = | permeability of free space                     |
| $\omega$      | = | wave angular frequency                         |
| $\omega_{ce}$ | = | electron cyclotron frequency                   |
| $\omega_{ci}$ | = | ion cyclotron frequency                        |
| $\omega_{pe}$ | = | electron plasma frequency                      |

## I. Introduction

Hall effect thrusters (HETs) can satisfy many of the current and future spacecraft propulsion needs of the United States Air Force (USAF). The USAF has recently identified high-power, bimodal HETs as the baseline approach for a variety of missions, including LEO-to-GEO orbit transfer vehicles, space tugs, servicing/re-supply vehicles for large orbital assets, e.g. Space Based Laser, and station-keeping. In the first mode, the thruster operates at low specific impulse ( $I_{sp}$ ) and a high thrust-to-power ( $T/P$ ) ratio to reduce the transfer time of large delta-V maneuvers. In the second mode, the HET operates at high specific impulse and low thrust for station keeping. To date, the low  $I_{sp}$  and high thrust mode is unattainable with standard HET configurations. The performance of the HET is limited in part by the efficiency of the electron bombardment process used to ionize the propellant. These limitations become especially pronounced at the low discharge voltages required to achieve high  $T/P$  ratios, i.e., conditions where a significant fraction of the input power is used to ionize the propellant.

Thus, to further improve the efficiency and achieve the required  $T/P$  ratio, a more efficient ionization technique must be used. One concept for achieving significant increases in efficiency at low discharge voltages is to replace the electron bombardment process with a helicon plasma source – a high-density, high-efficiency RF plasma source, which is possibly the most efficient method for creating high-density, low-temperature plasma. Cylindrical helicons are capable of producing plasmas with the density required to achieve high  $T/P$  ratios in HETs, but their geometry is not readily incorporated into the annular HET discharge chamber. However, an annular helicon plasma source could feed directly into the rear of the HET discharge chamber.

Yano and Walker<sup>1-3</sup>, in parallel with Beal et al<sup>4</sup> have shown that it is possible to develop an annular helicon

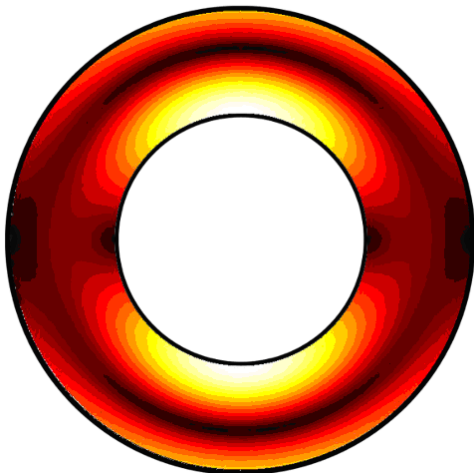


**Figure 1. The electric field pattern for the  $m = 1$  mode.** Lighter color represents the region of strong electric field, and darker color represents the region of weak electric field.

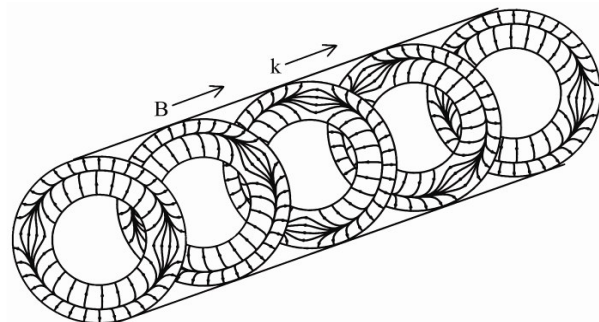


**Figure 2. Electric field pattern rotates both spatially and with time in the  $m = 1$  mode.** The wave propagates in the direction of the applied field.

plasma source that could feed directly into the HET discharge channel. In addition, Yano has derived the general helicon dispersion relation for an annular source, identified the first mode shape, performed power deposition calculations, and conducted some of the parametric studies.<sup>1</sup> The same assumptions used to derive the dispersion relationship for a cylindrical source, which has been experimentally verified, are used for the annular configuration. The equations are solved numerically to obtain the perturbed electric and magnetic field shapes and thus the mode shapes, which resulted in a general solution applicable for annularly bounded helicons. The work proves that an RF antenna can theoretically excite a helicon wave in annularly-bounded magnetized plasma.

The annular helicon scaling parameters derived with dispersion relations for non-uniform density plasmas will be compared to the experimental data as a part of this effort. In addition, comparisons are made between experimental results and inputs used for the current wave field simulation in an attempt to validate the assumptions used therein. Additionally, profiles of electron temperature and number density have been constructed according to RF input power.

## II. Helicon Dispersion Relation

Helicon waves are bounded whistler waves with frequencies between the ion and electron cyclotron frequencies such that

$$\omega_{ci} \ll \omega \ll \omega_{ce} \quad (1)$$

where  $\omega_{ci}$  and  $\omega_{ce}$  are the ion and electron cyclotron frequencies respectively. In this range of frequencies, we may safely assume that electron cyclotron motion is too fast to matter, and so only their guiding center drift is kept, and that ion cyclotron motion is so slow that ions may be treated as stationary. We also assume that plasma resistivity is zero.

The helicon dispersion relation was previously derived by Chen<sup>5</sup>, and that derivation is partially reproduced here. We begin with the following three linearized equations:

$$\nabla \times \mathbf{E} = -\frac{\partial \mathbf{B}}{\partial t} \quad (2)$$

$$\nabla \times \mathbf{B} = \mu_0 \mathbf{j} \quad (3)$$

$$\mathbf{E} = \frac{\mathbf{j} \times \mathbf{B}_0}{en_0} \quad (4)$$

where  $\mathbf{E}$ ,  $\mathbf{B}$ , and  $\mathbf{j}$  are the perturbed electric field, magnetic field, and current density, and  $\mathbf{B}_0$  and  $n_0$  are the equilibrium magnetic field and plasma density, respectively. These equations can be rearranged into

$$\nabla \cdot \mathbf{B} = 0 \quad (5)$$

$$\nabla \cdot \mathbf{j} = 0 \quad (6)$$

$$j_{\perp} = -\frac{en_0 \mathbf{E} \times \mathbf{B}_0}{B_0^2} \quad (7)$$

We now apply RF perturbations of the form

$$\mathbf{B} = \mathbf{B}(r) e^{i(m\theta + kz - \omega t)} \quad (8)$$

where  $m$  is the azimuthal mode number,  $k$  is the parallel wave number, and  $\omega$  is the angular frequency of the perturbation. Then Eqs. (2), (3), and (4) lead to

$$\nabla \times \mathbf{B} = \frac{\omega e n_0 \mu_0}{k B_0} \mathbf{B} \quad (9)$$

To simplify this expression, we define

$$\alpha = \frac{\omega \mu_0 e n_0}{k B_0} = \frac{\omega \omega_{pe}^2}{k \omega_{ce} c^2} \quad (10)$$

where  $\omega_{pe}$  is the electron plasma frequency. Substituting Eq. (10) into Eq. (9) yields

$$\nabla \times \mathbf{B} = \alpha \mathbf{B} \quad (11)$$

which illustrates an important result. We may substitute Eq. (11) into Eq. (3) to yield

$$\mathbf{j} = \frac{\alpha}{\mu_0} \mathbf{B} \quad (12)$$

We may also take the curl of Eq. (11) to obtain

$$\nabla^2 \mathbf{B} - \alpha^2 \mathbf{B} = 0 \quad (13)$$

This is the Helmholtz differential equation which governs the behavior of helicon waves and, together with Eq. (11) describes a key element in their shape: the perturbed magnetic field is everywhere parallel to its own curl. Imagine a single magnetic field line surrounded by others in such a way that the curl on that field line is parallel to it. To illustrate the required shape of the field, let there be a circular disk perpendicular to that field line of some small radius, as shown in Fig. 3(a). At the perimeter of that disk, the next field line must be oriented in such a way that it has an azimuthal component with respect to that first field line. This is the beginnings of a helix. Since the curl along that field line must be everywhere equal, each field line must be the center of a helix. One possible shape which satisfies this condition is a set of concentric helices of pitches which decrease as radius increases, as shown in Fig. 3(b).

The solution to Eq. (13) is the helicon dispersion relation:<sup>5</sup>

$$\frac{B_0}{n_0} = \frac{e \mu_0 a}{Z_m} \left( \frac{\omega}{k} + \frac{\omega a}{m Z_m^2} \right) \quad (14)$$

Yano has developed a computer simulation of the annular helicon wave field based on Eq. (14) and presented those results previously.<sup>2,3</sup> The simulation requires several estimated parameters and assumptions, among them being the radial plasma number density profile, and the assumption that power coupling into the plasma is helicon wave mode coupling and not predominately capacitive or inductive in nature.

The current investigation has produced data from RF-compensated and uncompensated Langmuir probes,<sup>6</sup> from which the electron temperature and number densities are calculated to provide initial validation of some the assumptions made in Yano's simulation inputs. We now compare results drawn from this data to the theory and model discussed above.

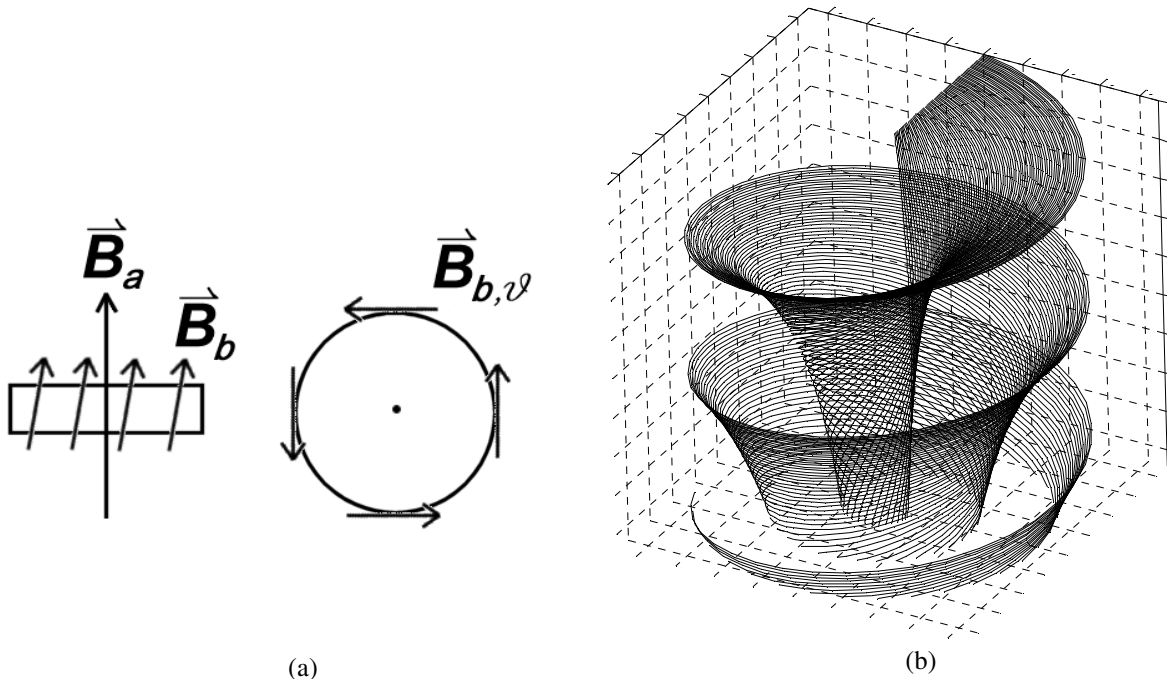


**Figure 3. The perturbed magnetic field of a helicon wave.** (a) For the curl of the field to be parallel to a given field line,  $\mathbf{B}_a$  at any point, nearby field lines,  $\mathbf{B}_b$ , must have an azimuthal component,  $\mathbf{B}_{b,\vartheta}$ , with respect to that field line, and thus form a helix around it. (b) For this to be true at all points throughout the field, the resulting structure must be a series of concentric helices of varying pitch.

### III. Experimental Apparatus

#### A. Vacuum Test Facility

Experiments are conducted in the Georgia Tech Vacuum Test Facility (VTF). The VTF consists of a stainless steel cylindrical vacuum chamber 7 m long and 4 m in diameter with six 48" diffusion pumps with a total pumping speed of 600,000 l/s on air at a base pressure of  $7.5 \times 10^{-6}$  Torr.<sup>6</sup>

#### B. Annular Helicon

The helicon device used for these experiments is shown in Fig. 4. The main vessel consists of two concentric Pyrex tubes 48" in length. The inner tube has an outer diameter of 120 mm, and the outer tube has an inner diameter of 171 mm, nominally. There are two Nagoya III antennas surrounding the annular region, shown in Fig. 5, as well as five 300-turn magnetic coils capable of generating magnetic fields up to approximately 450 G. Argon is fed into the closed end of the device and passed between the antennas. The RF system delivers from 50 W to 1 kW to the annular region through the two antennas.

RF power is supplied by a Yaesu FT-540 HF transceiver connected to an ACOM 2000A linear amplifier and a Palstar AT5K 3500 W T-matching network. This system can deliver in excess of 1 kW forward power at 13.56 MHz with less than 5 W reflected.<sup>6</sup>

Diagnostic probes are inserted through the open end of the device. These include several custom-built Langmuir probes, as well as custom-built magnetic field probes to measure electron number density and perturbed magnetic field fluctuations, respectively.



**Figure 4.** The annular helicon mounted inside the VTF.

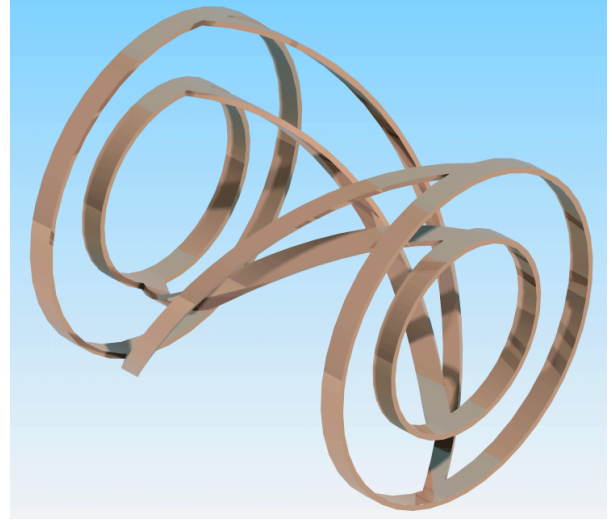


**Figure 5.** The dual, Nagoya-III helical antennas. The smaller antenna sits inside the inner tube, and the outer antenna on the outside of the outer tube so that neither is in direct contact with the main body of plasma in the annulus.

#### IV. Langmuir Probe Analysis

In this analysis, we use Orbital Motion Limited (OML) theory to analyze Langmuir probe data, which assumes that charged particles have some angular momentum with respect to a probe before they encounter its sheath and thus orbit the probe in either open or closed trajectories.<sup>7</sup> At high enough probe bias potentials, all electrons entering the probe sheath are collected. We call that potential the electron saturation current,  $I_{es}$ .

Electron temperature is determined by the rate at which probe current increases as bias potential increases using<sup>8</sup>

$$T_e = \frac{dV_p}{d(\ln I_p)} \quad (15)$$

where  $V_p$  is the probe bias voltage,  $I_p$  is the probe current in Amperes, and  $T_e$  is in electron-volts, over a linear fit in the transition region as shown in Fig. 6. The electron number density may then be calculated by the empirical formula<sup>9</sup>

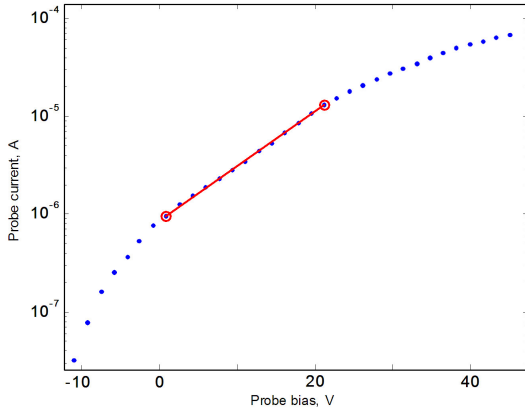


**Figure 6.** Example semilog plot of the I-V characteristic of a Langmuir probe in an RF plasma and the linear fit. The region of best linear fit is estimated, and the slope at that region used to calculate the plasma characteristics.

$$n_e = 3.73 \times 10^{13} \frac{I_{es}}{A_p \sqrt{T_e}} \quad (16)$$

where  $A_p$  is the probe collection area.

A key parameter in determining the applicability of the various Langmuir probe theories is the ratio of probe radius to Debye length, given by

$$\beta = \frac{r_p}{\lambda_D} = \sqrt{\frac{r_p^2 n_0 e^2}{\epsilon_0 T_e}} \quad (17)$$

Generally, the applicability of OML theory is limited to cases where  $\beta < 3$ .<sup>8</sup> In our case, this parameter varies substantially, depending on the electron temperatures calculated, which range from 5 eV to 40 eV.

## V. Results and Discussion

Analysis of the Langmuir probe data involves substantial ambiguity in the determination of the proper curve fit in the transition region necessary to calculate the electron temperature. Clearly defined linear regions of data are not always visible on either raw data or data corrected for the ion current contribution in the transition region. Figure 7 depicts one of the cases where the linear region on the semilog plot is reasonably well defined between approximately 10 and 40 V. Still, we do recognize that a space potential of 40 V is abnormally high and are as of yet unable to explain why this is observed. Equally surprising is the high electron temperatures this analysis produces from the data. The case shown in Fig. 7 produces an electron temperature of 16.1 eV, which is substantially higher than cylindrical helicons reported in existing literature

Our results are disproportionate when compared to those of cylindrical helicons in similar operational regimes.<sup>10</sup> These devices operate in the helicon wave power coupling modes, which provides an order of magnitude higher plasma density than inductive modes.<sup>5</sup> These devices are generally more compact, and operate with higher input power and neutral density than those available in our experimental apparatus.

Additionally, our data strongly suggests that power coupling into the annular helicon plasma is inductive in nature. Yet, depending on the subjectivity inherent in the Langmuir probe analyses, the same data also suggests that our electron number densities and temperatures are well above those of the cylindrical helicons operating in the more efficient helicon wave mode. Thus the magnitude of our results is inconsistent with expectation. Still, the trends visible in our data are, where clearly visible, consistent with theory and established trends. In particular, the radial profile of electron density shown in Fig. 8 suggests that the theoretical profile utilized in the Yano wave field model is of the right shape.

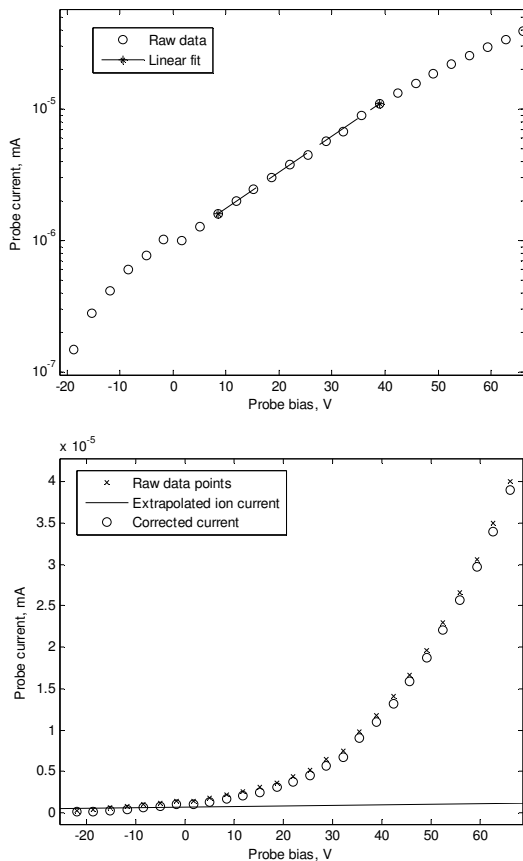


**Figure 7. Linear and semilog I-V characteristics of a Langmuir probe in the annular helicon.** Forward RF power of 1 kW is supplied at 13.56 MHz, with a flow of argon of 100 sccm at a facility operating pressure of  $2.5 \times 10^{-5}$  Torr.

The difference between the observed and assumed radial density profiles is noteworthy. Based on the calculated electron temperature and densities using OML, the density peaks in a very narrow region around the center of the annular channel and in a manner far steeper than the assumed profile. This cannot be the beginnings of the sheaths at the boundaries, as these are at most several Debye lengths thick, and the Debye length in this plasma is orders of magnitude smaller than this distance. Clearly, the observed trend differs from the assumed profile near the walls. The density drops off rapidly very near the center of the annulus and remains nearly constant at a lower level to the edge of the measurable radial distance. Physical limitations in the apparatus

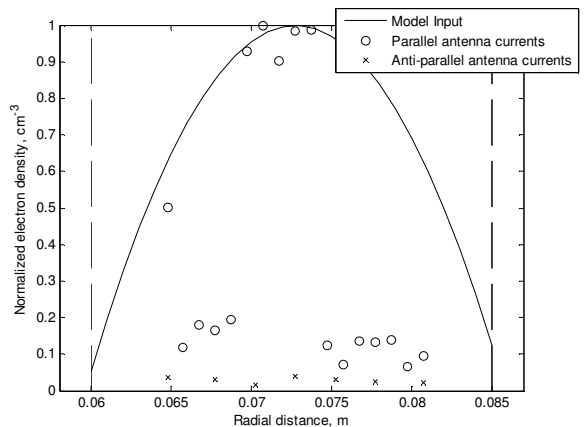


**Figure 8. Estimated and experimentally derived radial electron density profile for two different antenna configurations.** The annulus walls are at  $r = 0.06$  and  $0.085$  m. Experimental points are normalized by the peak density in the parallel antenna currents

prevent measurement closer to the walls as the probe is inserted axially through the open end of the annular channel.

Of the other profiles measured, the most noteworthy is the profile of electron number density with respect to RF power shown in Fig. 9. The two profiles were measured with the antennas connected differently. First, a set of measurements is taken with the antenna currents parallel to one another. Then, a second set is taken after one pair of the RF feedlines outside the vacuum chamber was reversed so that the antenna currents flowed anti-parallel to one another. This agrees well with expectations in that both profiles show a clear step increase in density at a given RF power: 300 W for the parallel current, and 550 W for the anti-parallel current.

This jump is consistent with those observed by Chi, Sheridan and Boswell<sup>10</sup> in their ion saturation currents as their plasma transitioned between the various power coupling modes. However, even if we conclude that this is a power coupling mode transition, at best, step changes in density serve only as circumstantial evidence of power coupling mode. Ultimately, the true mode can only be determined by sampling the wave field.

We note that there is no major change in the plasma impedance throughout the power range in question, as determined by the optimal matching network settings required to minimize reflected power. This observation, together with the fact that 100-300 W is required to ignite the plasma (depending on antenna current orientation), suggests that this jump is the transition from the capacitive power coupling mode to the inductive mode.

## VI. Conclusion

The observed radial density profile is largely consistent with what one would expect in an annular channel like that in the annular helicon. The power density profile also follows logical trends. The trends evident in the data at hand are generally consistent with existing theory and other experimental data. However, if the magnitudes of the electron temperatures and number densities are accurate, then one would have to conclude that a large part of the operating regime explored is within the helicon wave coupling mode. Simultaneously, the power profile implies that the device operates in the inductively-coupled mode, but electron temperatures and densities of this magnitude have never been measured in cylindrical helicons, even when operating in the more efficient helicon wave mode, much less the inductive mode.

The next step is to sample the wave field and make comparisons to the available theoretical and experimental data. In addition, the development of a discharge equilibrium model will allow for experimental confirmation of power coupling modes with Langmuir probe data.

## Acknowledgements

The authors wish to thank the other graduate and undergraduate researchers in the High-Power Electric Propulsion Laboratory at Georgia Tech who have provided substantial support of this work, and Andrew Carignan, Scott Moseley, and Scott Elliott of the Aerospace Engineering machine shop. This research is supported by the Air Force Office of Scientific Research grant FA9550-07-1-0137. Dr. Mitat Birkan is the contract monitor.

## References

1. Yano, M., Walker, M. L. R., "Plasma Ionization by Annularly-Bounded Helicon Waves," *Physics of Plasmas*, Vol. 13, No. 6, 2006, pp. 063501.
2. Yano, M., Palmer, D., Williams, L., Walker, M. L. R., "Design and Operation of an Annular Helicon Plasma Source," AIAA 2007-5309, *43rd Joint Propulsion Conference*, Cincinnati, OH, July 8-11, 2007.
3. Yano, M., Walker, M. L. R., "Generalized Theory of Annularly Bounded Helicon Waves," *Physics of Plasmas*, Vol. 14, No. 3, 2007, pp. 033510.

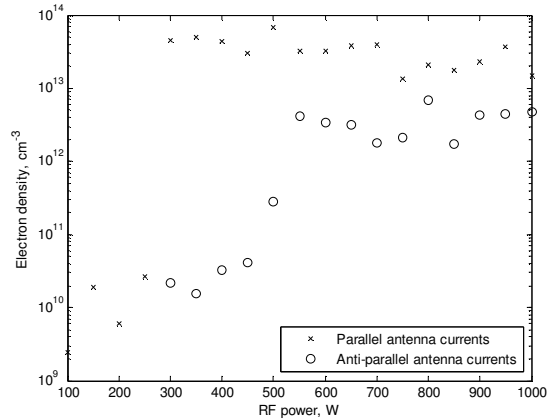


Figure 9. Electron density power profile with antenna currents running parallel and anti-parallel.

4. Brian E. Beal, A.D.G., David P. Morris, Christopher Davis, Kristina M. Lemmer, "Development of an Annular Helicon Source for Electric Propulsion Applications," *42nd AIAA/ASME/SAE/ASEE Joint Propulsion Conference & Exhibit*. 2006-4841, AIAA: Sacramento, CA, 2006.
5. Chen, F.F., "Plasma Ionization by Helicon Waves," *Plasma Physics and Controlled Fusion*, Vol. 33, No. 4, 1991, pp. 339-364.
6. Palmer, D., Akinli, C., Walker, M.L.R., "Characterization of an Annular Helicon Plasma Source," *International Electric Propulsion Conference*, 2007-202, Florence, Italy, 2007.
7. Chen, F.F., "RF Langmuir Probes, revisited," in *58<sup>th</sup> Gaseous Electronics Conference*. 2005: San Jose, CA.
8. Chen, F.F., "Langmuir Probe Diagnostics," *IEEE-ICOPS*. 2003: Jeju, Korea.
9. Hiden, "*Handbook of Plasma Diagnostics*," Warrington, England.
10. Chi, K., Sheridan, T.E., Boswell, R.W., "Resonant Cavity Modes of a Bounded Helicon Discharge," *Plasma Sources Science and Technology*, Vol. 8, 1998, pp. 421-431.
11. Sudit, I.D., Chen, F.F., "RF Compensated Probes for High Density Discharges," *Plasma Sources Science and Technology*, 1994. **3**: p. 162-168.